sciendo

PRODUCTION ENGINEERING ARCHIVES 2020, 26(4), 167-173

PRODUCTION ENGINEERING ARCHIVES

ISSN 2353-5156 (print)
ISSN 2353-7779 (online)

Exist since 4th quarter 2013
Available online at https://pea-journal.eu

Effect of non-zero mean stress bending-torsion fatigue on fracture surface parameters of 34CrNiMo6 steel notched bars

Wojciech Macek[1*], Mirosław Szala[2], Jarosław Trembacz[3], Ricardo Branco[4], José Costa[4]

[1] University of Occupational Safety Management, Bankowa 8, 40-007 Katowice, Poland,
[2] Lublin University of Technology, Faculty of Mechanical Engineering, Nadbystrzycka 36D, 20-618 Lublin, Poland,
[3] Opole University of Technology, Prószkowska 76, 45-758 Opole, Poland
[4] University of Coimbra, CEMMPRE, Department of Mechanical Engineering, Coimbra, Portugal,
*Corresponding author e-mail: wojciech.macek@yahoo.com

Article history
Received 03.10.2020
Accepted 18.11.2020
Available online 31.12.2020

Keywords
multiaxial fatigue
bending-torsion
notch effect
fatigue fracture
surface topography

Abstract
Modern methods of testing materials require the use of the latest technologies and combining measurement and calculation methods. It is important to find a quantitative way of describing, among other things, the failures so that it can help to design with high accuracy. This paper studies loading orientations on crack shape and fracture surface changes. The advantage of the entire fracture surface method is simplicity and applicability in studies on other materials, shapes and loadings. A higher values of fracture surface parameters (Sx, Vx) was observed in failure specimens with lower σ/τ (B/T) ratios. It has been observed that largest crack lengths with a small number of cycles occur for loading combinations different then B=T. As well as analyzed surface parameters Sx, Vx, are higher for larger number of cycles to crack initiation (Ni) values.

DOI: 10.30657/pea.2020.26.30

JEL: L69, M11

1. Introduction

Engineering materials with different geometries and shapes are with their nuances increasingly reflected in fatigue tests (Kowal and Szala, 2020; Ulewicz et al., 2014; Ulewicz et al., 2019; Trško et al., 2020; Wu et al., 2020; Robak, 2020). Loading generation also needs to be developed to get as close as possible to the service conditions, both by standard and a special performance of fatigue machines (Jamali et al., 2019; Rozumek et al., 2018; Saito et al., 2020; Pejkowski et al. 2018). Fatigue and Fracture of metals under bending with torsion loading have been studied by authors of this work (Branco et al., 2018; W. Macek et al., 2020). Similar studies were rarely carried out in the past, but for bending-torsion fatigue studies we would like to mention the publications (Böhm et al., 2015; Carpinteri et al., 2008; Rozumek et al., 2018; Singh et al., 2019; Slámečka et al., 2010; Lachowicz and Owsiński, 2020). Singh et al. (Singh et al., 2019) and Susmel with Petrone (Susmel and Petrone, 2003) also analyzed this type of loading for fatigue crack initiation and propagation behavior. Pawliczek and Prażmowski (Pawliczek and Prażmowski, 2015) have tested S355 steel specimens with mean block bending loadings. Samples after fatigue tests were subjected to metallographic examinations. These papers show how important it is to look at the surface and morphology of material in different scales, e.g. from nano- to macro-scale.

The application of metrological technologies and techniques to understand the fracture mechanisms of studied materials have expanded along with the development of measuring technologies, as noted by among others, Jollivet and Greenhalgh (Jollivet and Greenhalgh, 2015) in composite materials, as well as Goldsmith et al. (Goldsmith et al., 2019) for in-service aircraft crack research, respectively. Vanderesse et al (Vanderesse et al., 2020) have used three techniques for evaluating the fracture mechanisms, as X-ray computed tomography (XCT), laser scanning confocal microscopy (LSCM), and scanning electron microscopy (SEM). Their studies were conducted for pre-mortem and post-mortem characterizations. Sinha et al. (Sinha et al., 2020) have used X-ray microscopy to examine specimens subjected to tension and found that microstructural flexibility induced different tendencies for void

growth and ductile fracture mode. Also optical and laser apparatus for areal surface topography investigation, that allow measure at broad range of scales, are becoming more and more popular. This is recognized and conconcluded by Feng et al (Feng et al., 2019) as well as Senin et al. (Senin et al., 2017) on the example of optical technologies measurements covered, among others, by imaging confocal microscopy (ICM), chromatic confocal microscopy, phase shifting interferometry, coherence scanning interferometry (CSI), point autofocus instruments (PAI), and focus variation microscopy (FVM). Stemp et al. (Stemp et al., 2019) and also Macek et al. (Macek et al., 2020a) used FVM measurement systems for their research on stone tools and fracture surfaces, respectively.
Fonte et al. (Fonte et al., 2007) showed results for the fatigue crack surface roughness Ra and Rz according to ISO 4287 (ISO, 1997) with the fatigue crack propagation direction at the center of fracture surface. Although similar roughness results were achieved at the center and at the both sides of the fracture, areal surface Sx parameters according to ISO 25178 (ISO, 2012; Arsalani et al., 2020; Yang et. al., 2019) give complete information because a single line cannot identify pits or valleys and show the relationship between surface function, as confirmed by Stach et al. (Stach et al., 2017). The combination of fatigue testing with the surface metrology by the authors of this work (Macek, 2019a, 2019b) gave promising results in previous studies. Therefore, it was decided to develop this methodology, based on the entire fracture surface, for testing other materials subjected to bending with torsion.

2. Experimental

2.1. Material

The fracture analysis and the fatigue tests were done using cylindrical specimens (see Fig. 1) made of low alloy steel grade 34CrNiMo6 (Szala, 2017). The samples were oil quenched and tempered according to the procedure described elsewhere (Branco et al., 2016). The chemical composition and the main mechanical properties are shown in Tables 1 and 2, respectively.

Table 1. Nominal chemical composition (wt%) of DIN 34CrNiMo6 steel (Branco et al., 2016)

C	Si	Mn	Cr	Mo	Ni
0.34	≤ 0.40	0.65	1.50	0.22	1.5

Table 2. Mechanical monotonic properties of the DIN 34CrNiMo6 steel (Branco et al., 2016)

Mechanical property	Value
Yield strength, σ_{YS} (MPa)	967
Tensile strength, σ_{UTS} (MPa)	1035
Young's modulus, E (GPa)	209.8
Poisson's ratio, ν	0.296

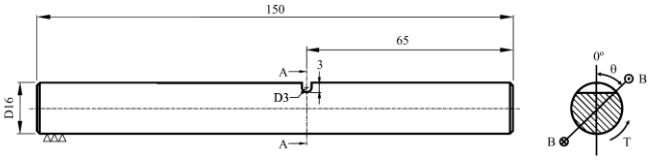

Fig. 1. Specimen geometries (in millimetres)

2.2. Methods

2.2.1. Fatigue test

The fatigue tests were carried out using the fatigue test stand exhibited in Fig. 2. The tests were conducted under constant amplitude loading with three ratios of the bending moment (B) to torsion moment (T), more precisely B/T=2, B/T=1, and B/T=2/3. Three orientations of the bending moment with respect to the notch geometry were considered (see Fig. 1), i.e. θ=0º, 45º, and 90º. A stress ratio equal to 0 was used.

Fig. 2. Fatigue test stand with own-made gripping system

2.2.2. Fracture surface measurement

The measurements of surface topography were undertaken through the InfiniteFocus G4, with a FVM technology by Alicona, which was placed on the antivibration table (see Fig. 3).

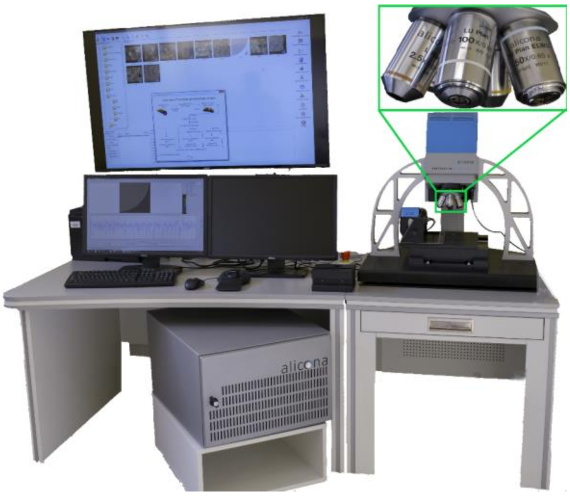

Fig. 3. FVM Alicona G4 setup

The scanned surfaces, whose textures can be seen in Annex A, have been extracted to the form exhibited in Figure 4. The individual steps for cutting the proper surface are also shown in the first fragment of Figure 6.

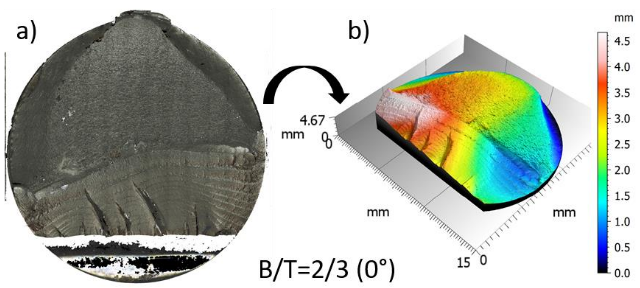

Fig. 4. Fracture texture visualization a) original merged photo, b) extracted colour simulation

3. Theory and calculation

3.1. Fatigue parameters

In the fatigue tests, the crack length was evaluated at periodic intervals varying between 2000 and 10,000 cycles using a high-resolution digital camera. The number of cycles to crack initiation was defined from the curves relating the surface crack length with the number of cycles for a crack length equal to the characteristic material length, a_0 = 129 μm.

3.2. Surface parameters and their definitions

For the purposes of checking the fracture surface dependency on the fatigue loading history, selected parameters were measured and calculated. Table 3 defines the parameters used in this paper which were selected according to ISO 25178 standard.

Height parameters are a class of surface parameters that quantify the Z-axis perpendicular to the surface. They are included in the ISO 25178 standard. The reference plane for the calculation of these parameters is the mean plane of the measured surface.

Table 3. Selected parameters for the fatigue fracture surface description according to ISO 25178

Height parameters			
Sq	μm	Root-mean-square height	$Sq = \sqrt{\frac{1}{A}\iint_A z^2(x,y)dxdy}$
Ssk		Skewness	$Ssk = \frac{1}{Sq^3}(\frac{1}{A}\iint_A z^3(x,y)dxdy)$
Sku		Kurtosis	$Sku = \frac{1}{Sq^4}(\frac{1}{A}\iint_A z^4(x,y)dxdy)$
Sp	μm	Maximum peak height	Sp = Sz – Sv
Sv		Maximum pit height	
Sz		Maximum height	Height between the highest peak and the deepest valley
Sa		Arithmetical mean height	Mean surface roughness $Sa = \frac{1}{A}\int_A \lvert z(x,y)\rvert dxdy$
Functional Parameters (Volume)			
Vm	$\frac{mm^3}{mm^2}$	Material volume	
Vv		Void volume	
Vmp		Peak material volume	
Vmc		Core material volume	
Vvc		Core void volume	
Vvv		Pit void volume	

Functional parameters (Volume) Vx represent an evolution of the functional indices and are defined, like the family of Sx parameters. A graphical interpretation of functional parameters is presented on the Abbott curve represented in Fig. 5 (Abbott and Firestone, 1933; Kaplonek et al., 2016).

Both sides of specimens are fixed to the grips, but both move during the tests. One side rotates, and the other one has rotation and translation movements. The side which was measured and analysed corresponds to the former case. Skewness Ssk means the absence of symmetry distribution, and kurtosis Sku indicates how the results obtained are arranged in relation to the normal distribution.

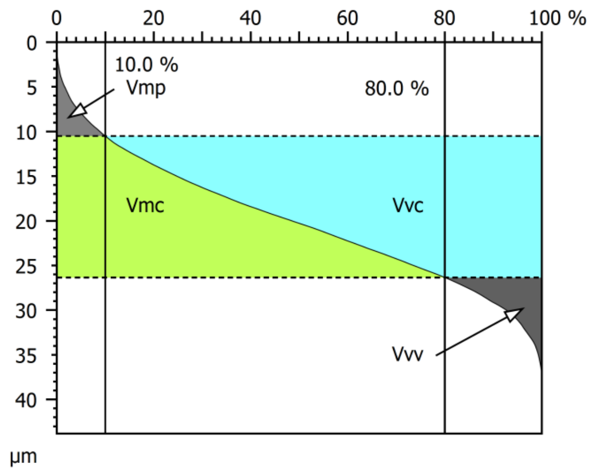

Fig. 5. Example of the Abbott curve with selected Functional Parameters (Volume), Vx

4. Results

The methodology of extracting areas and selected results obtained for the fatigue fracture surface by the InfiniteFocus® IF G4 focus variation microscope during the experimental investigations is graphically presented in Fig. 6. All 3D parameters have been calculated on the whole current surface, as marked in Fig. 6. The whole current surface was reduced to eliminate the final break, discontinuities and "non-sampling" areas.

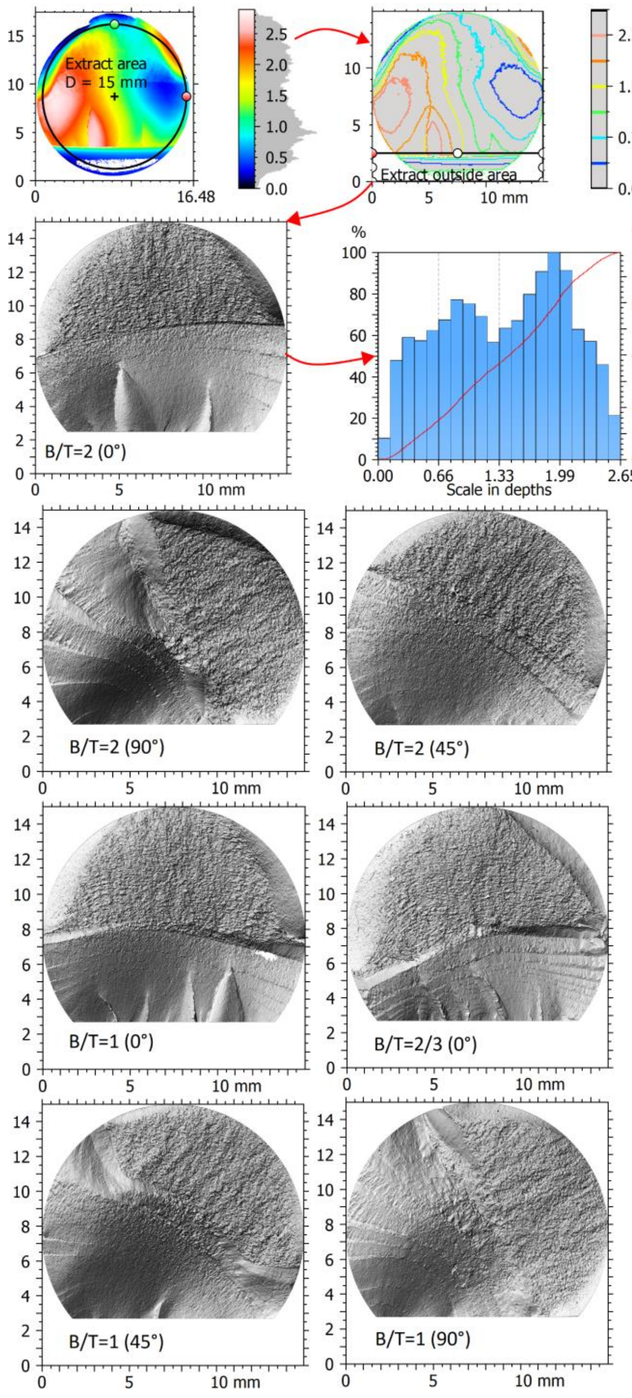

Fig. 6. The whole current reduced surfaces

The effect of B/T ratio on height parameters Sx is shown in Figures 7 and 8. The effect of B/T ration on functional (volume) Vx parameters is displayed in Figure 9. For the sake of clarity, the B/T ratios are accounted for in terms of normal stress to shear stress ratios (σ/τ), i.e. σ/τ = 2, σ/τ = 4, σ/τ = 4/3, which correspond to B/T=2, B/T=1, and B/T=2/3, respectively.

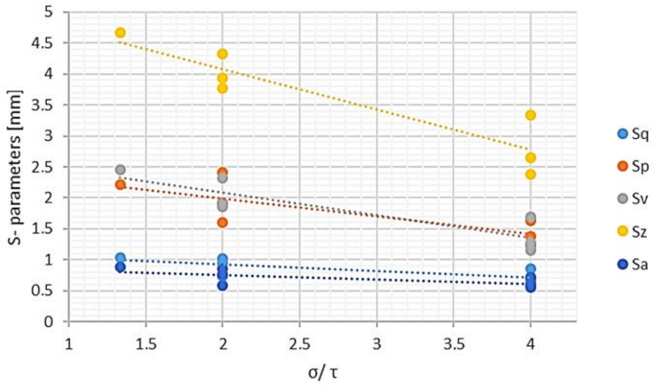

Fig. 7. Height parameters Sx of the investigated fracture surfaces for different bending-torsion ratios

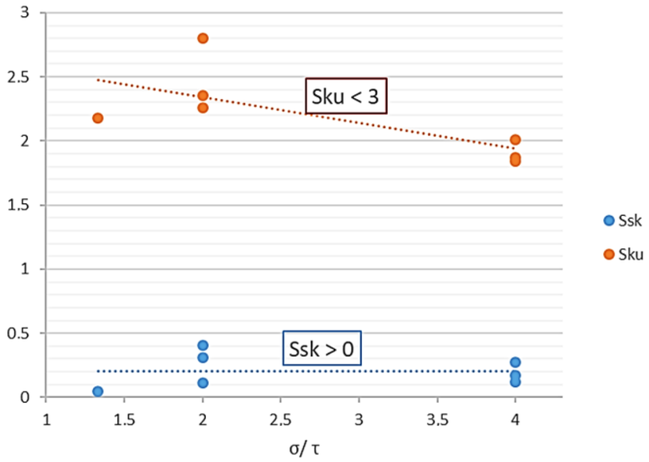

Fig. 8. Kurtosis Sku and skewness Ssk of the investigated fracture surfaces for different B/T ratios

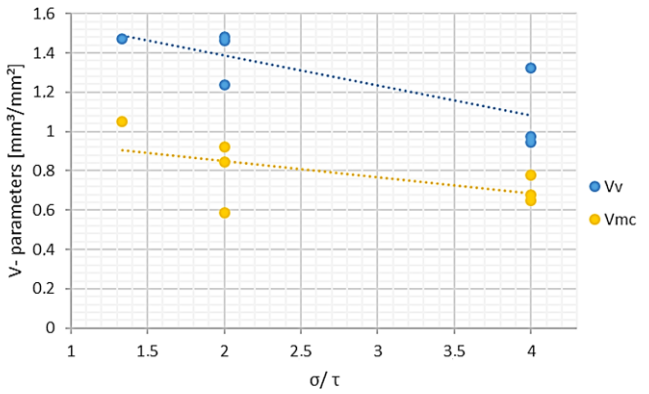

Fig. 9. Functional parameters (volume) for investigated fracture surfaces

Generally, positive Ssk indicates the presence of more peaks, while negative Ssk shows the presence of more valleys; a Ssk value close to zero indicates symmetrical distribution of surface irregularities. The normal value distribution has a Sku value equal to 3. The Sku parameter reveals the presence of excessively high peaks or deep valleys on the surface for Sku > 3, and lack of these features for Sku < 3.

The same parts of the sample (grip side) were used for the study of surface topography, which is confirmed by the results. All Ssk values were positive, which indicates the predominance of peaks on the surface. While all Sku values were less than 3 what is related to the absence on the surface of inordinately high peaks or deep valleys.

There is a linear relationship with the σ/τ (B/T) ratio for both the Sx and Vx parameters presented in Figures 7 and 9, respectively.

Figure 10 presents crack length 2b relative to number of cycles N for different loading scenarios.

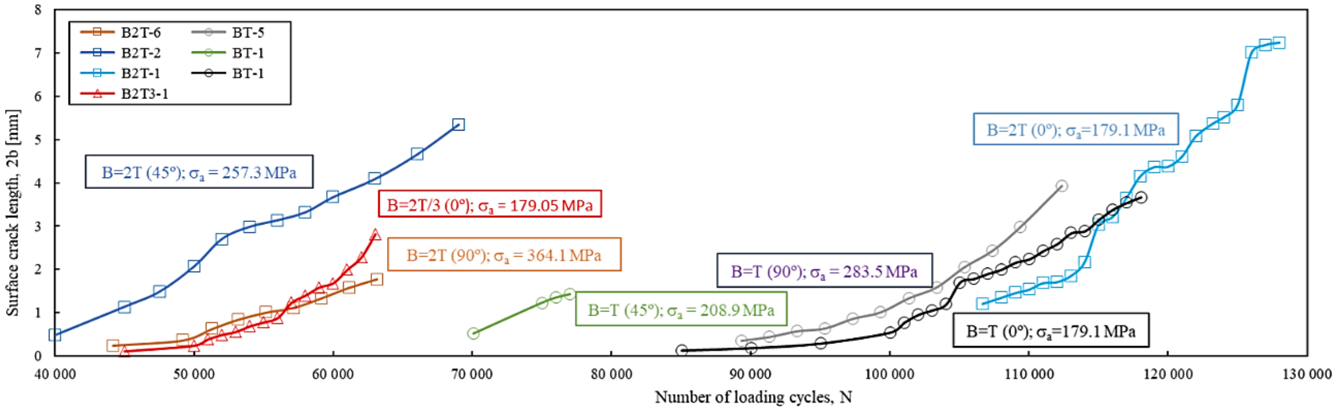

Fig. 10. Crack length 2b vs. Number of cycles N

5. Discussion

Fig. 11 shows the number of cycles to crack initiation Ni vs. surface roughness parameters Sa and Vv. The surface parameters Sa and Vv were selected from the group Sx and Vx, respectively, as the most representative. Analyzing the results of experimental tests shown in the diagram, one can see that the values of both Sa and Vv are higher for larger number of cycles to crack initiation Ni values. Smaller values, for both surface parameters and the number of cycles, occur for B/T=2 loadings, while for the other loading combinations the values tend to be higher.

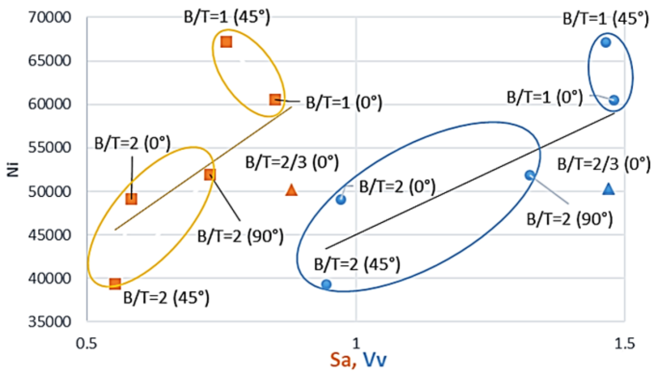

Fig. 11. The number of cycles to crack initiation Ni in function of surface roughness parameters Sa and Vv for different loading cases

Figure 12 presents selected surface fracture parameters (Sa, Vv) in function of the bending moment angle and the bending-torsion ratio. It is a box and whisker chart, where the mean marker of the selected series is shown as "x", and "o" represents the data points that lie between the lower whisker and the upper whisker lines. The median is excluded from the calculation if the number of values in the data is odd. The two boxplots, showing the average values of the surface parameters Sa and Vv from the bending-torsion ratio, display the same relationships. That is, the smallest average values of Sa and Vv occur for B/T=2, while the largest occur for B/T=2/3. However, the maximum values were found for two subsequent boxplots presenting the average values of the surface parameters Sa and Vv at a bending moment angle equal to 0 (i.e. θ=0°).

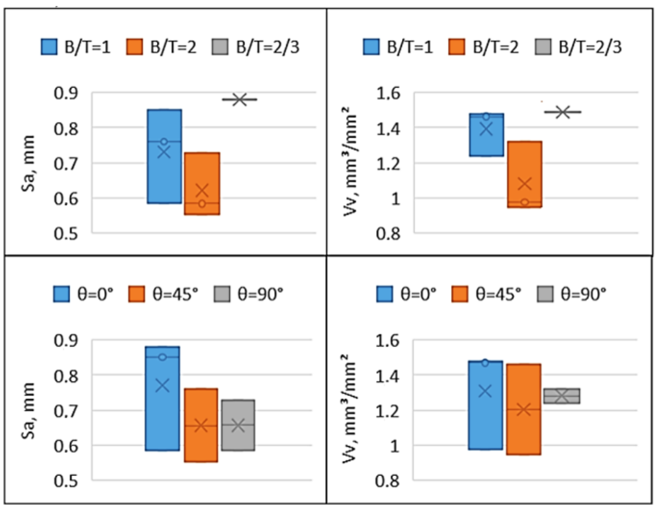

Fig. 12. Boxplot characterising Sa and Vv in the function of the bending moment angle θ and bending-torsion ratio

Surface parameters changes during the crack process do not influence the characteristics of the surface. This is clear by comparing the results of Sku–Ssk presented in Figure 13, since they are close which means that there was no change in configuration of parameters Sku and Ssk.

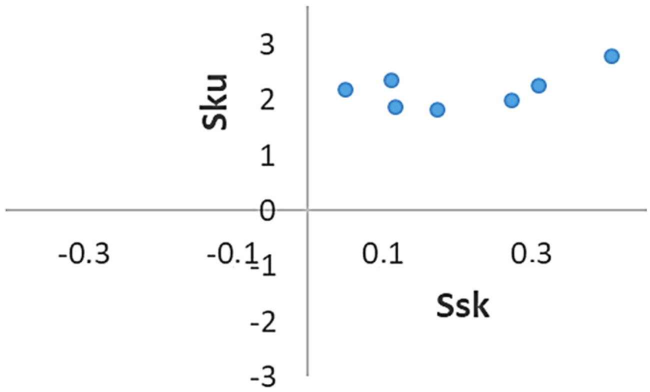

Fig. 13. The map of kurtosis (Sku) versus skewness (Ssk) for investigated fractures surfaces

As mentioned before, all Ssk values were positive, which indicates the predominance of peaks on surfaces. While all Sku values were less than 3 which is connected with the absence of inordinately high peaks or deep valleys on surfaces. Such high compliance results from the measurements of only one (the same) sides of broken specimens.

6. Conclusions

The presented analysis shows that the method used to measure the fatigue fracture is adequate for investigating fractures for a wide range of cases. The most significant results of this study can be presented as follows:

- The highest values of Sx and Vx occur for B/T = 2/3 and affects on smaller values for next both levels B/T=1 and B/T=2, respectively;
- High compliance of Ssk and Sku parameters proves the large dependence of these parameters on the grip side and, thus, the way it affects the material;
- Surface parameters (Sx, and Vx) are higher for higher values of the number of cycles to crack initiation (Ni);
- The smallest values of the number of cycles to crack initiation (Ni) and of the surface parameters (Sx, and Vx) were found for B/T=2;
- The largest values of the number of cycles to crack initiation (Ni) and of the surface parameters (Sx, and Vx) occurred for B/T=1;
- The two conclusions mentioned above confirm the dependence between the surface roughness and the bending-torsion ratio.

References

Abbott, E.J., Firestone, F.A., 1933. *Specifying surface quality*, Mech. Eng. 65, 569-572.

Arsalani, M., Razfar, M.R., Abdullah, A., Khajehzadeh, M., 2020. *Fatigue behavior improvement of hardened parts using sequential hard turning, grinding, and ball burnishing operations*, Proceedings of the Institution of Mechanical Engineers, Part L: Journal of Materials: Design and Applications.

Böhm, M., Kowalski, M., Niesłony, A., 2015. *Multiaxial fatigue test stand concept – Stand and control design*, Adv. Intell. Syst. Comput. DOI: 10.1007/978-3-319-10990-9_41

Branco, R., Costa, J.D., Berto, F., Antunes, F.V., 2017. *Effect of loading orientation on fatigue behaviour in severely notched round bars under non-zero mean stress bending-torsion*, Theor. Appl. Fract. Mech., 92, 185-197. DOI: 10.1016/J.TAFMEC.2017.07.015

Branco, R., Costa, J.D.M., Antunes, F.V., Perdigão, S., 2016. *Monotonic and cyclic behavior of DIN 34CrNiMo6 tempered alloy steel*, Metals (Basel). DOI: 10.3390/met6050098

Branco, R., Costa, J.D.M., Berto, F., Razavi, S.M.J., Ferreira, J.A.M., Capela, C., Santos, L., Antunes, F., 2018. *Low-cycle fatigue behaviour of AISI 18Ni300 maraging steel produced by selective laser melting*, Metals (Basel). DOI: 10.3390/met8010032

Carpinteri, A., Spagnoli, A., Vantadori, S., Viappiani, D., 2008. *A multiaxial criterion for notch high-cycle fatigue using a critical-point method. Eng. Fract*, Mech. DOI: 10.1016/j.engfracmech.2006.11.002

Feng, X., Senin, N., Su, R., Ramasamy, S., Leach, R., 2019. *Optical measurement of surface topographies with transparent coatings*, Opt. Lasers Eng. 121, 261–270. DOI: 10.1016/J.OPTLASENG. 2019.04.018

Fonte, M., Romeiro, F., Freitas, M., 2007. *Environment effects and surface roughness on fatigue crack growth at negative R-ratios*, Int. J. Fatigue 29, 1971-1977. DOI: 10.1016/J.IJFATIGUE.2007.02.027

Goldsmith, N.T., Wanhill, R.J.H., Molent, L., 2019. *Quantitative fractography of fatigue and an illustrative case study*, Eng. Fail. Anal. 96, 426-435. DOI: 10.1016/J.ENGFAILANAL.2018.10.013

International Organization for Standardization, 2012. *Geometrical product specifications (GPS) - Surface texture: Areal Part 2: Terms, definitions and surface texture parameters*, Int. Stand. ISO. DOI: 10.1136/ bmjopen-2015-009366

ISO 4287, 1997. *Geometrical Product Specifications (GPS) -- Surface texture: Profile method -- Terms, definitions and surface texture parameters*, Int. Organ. Stand. 25.

Jamali, J., Mahmoodi, M.J., Hassanzadeh-Aghdam, M.K., Wood, J.T., 2019. *A mechanistic criterion for the mixed-mode fracture of unidirectional polymer matrix composites*, Compos, Part B Eng. 176, 107316. DOI: 10.1016/J.COMPOSITESB.2019.107316

Jollivet, T., Greenhalgh, E., 2015. *Fractography, a Powerful Tool for Identifying and Understanding Fatigue in Composite Materials*, Procedia Eng. 133, 171-178. DOI: 10.1016/J.PROENG.2015.12.646

Kaplonek, W., Nadolny, K., Królczyk, G.M., 2016. *The use of focus-variation microscopy for the assessment of active surfaces of a new generation of coated abrasive tools*, Meas. Sci. Rev. DOI: 10.1515/msr-2016-0007

Kowal, M., Szala, M., 2020. *Diagnosis of the microstructural and mechanical properties of over century-old steel railway bridge components*, Eng. Fail. Anal. 110, 104447. DOI: 10.1016/J.ENGFAILANAL. 2020.104447

Lachowicz, C. T., Owsiński, R. 2020. *Comparative analysis of fatigue energy characteristics of S355J2 steel subjected to multi-axis loads*, Materials, 13(11) https://doi:10.3390/ma13112470

Macek, W., 2019a. *Post-failure fracture surface analysis of notched steel specimens after bending-torsion fatigue*, Eng. Fail. Anal. DOI: 10.1016/j.engfailanal.2019.07.056

Macek, W., 2019b. *Fractal analysis of the bending-torsion fatigue fracture of aluminium alloy*, Eng. Fail. Anal. 99, 97-107. DOI: 10.1016/ J.ENGFAILANAL.2019.02.007

Macek, Wojciech, Branco, R., Szala, M., Marciniak, Z., Ulewicz, R., Sczygiol, N., Kardasz, P., 2020a. *Profile and Areal Surface Parameters for Fatigue Fracture Characterisation*, Materials (Basel). 13, 3691. DOI: 10.3390/ma13173691

Macek, W., Branco, R., Trembacz, J., Costa, J.D., Ferreira, J.A.M., Capela, C., 2020. E*ffect of multiaxial bending-torsion loading on fracture surface parameters in high-strength steels processed by conventional and additive manufacturing*. Eng. Fail. Anal. 118. DOI: 10.1016/ j.engfailanal.2020.104784

Pawliczek, R., Prażmowski, M., 2015. *Study on material property changes of mild steel S355 caused by block loads with varying mean stress*, Int. J. Fatigue. DOI: 10.1016/j.ijfatigue.2015.05.019

Pejkowski, Ł., Skibicki D., Seyda J., 2018. *Stress-strain response and fatigue life of a material subjected to asynchronous loadings*, AIP Conference Proceedings 2028, 020016;
DOI: 10.1063/1.5066406

Robak, G., 2020. *Using a variable value of the fictitious radius to estimate fatigue life of notched elements*, Fatigue and Fracture of Engineering Materials and Structures, 43(9), 2006-2023. DOI: 10.1111/ffe.13280

Rozumek, D., Marciniak, Z., Lesiuk, G., Correia, J.A., de Jesus, A.M.P., 2018. *Experimental and numerical investigation of mixed mode I + II and I + III fatigue crack growth in S355J0 steel*, Int. J. Fatigue 113, 160-170. DOI: 10.1016/J.IJFATIGUE.2018.04.005

Saito, S., Ogawa, F., Itoh, T., 2020. *Investigation of fatigue strength under wide-ranged biaxial stress for two types of stainless steel using a thin-walled hollow cylinder specimen*, Int. J. Fatigue 105611. DOI: 10.1016/J.IJFATIGUE.2020.105611

Senin, N., Thompson, A., Leach, R.K., 2017. *Characterisation of the topography of metal additive surface features with different measurement technologies*, Meas. Sci. Technol. DOI: 10.1088/1361-6501/aa7ce2

Singh, A.K., Datta, S., Chattopadhyay, A., Riddick, J.C., Hall, A.J., 2019. *Fatigue crack initiation and propagation behavior in Al – 7075 alloy under in-phase bending-torsion loading*, Int. J. Fatigue 126, 346–356. DOI: 10.1016/J.IJFATIGUE.2019.05.024

Sinha, S., Nene, S.S., Frank, M., Liu, K., Lebensohn, R.A., Mishra, R.S., 2020. D*eformation mechanisms and ductile fracture characteristics of a friction stir processed transformative high entropy alloy*, Acta Mater. 184, 164–178. DOI: 10.1016/J.ACTAMAT.2019.11.056

Slámečka, K., Pokluda, J., Kianicová, M., Major, S., Dvořák, I., 2010. *Quantitative fractography of fish-eye crack formation under bending-torsion fatigue*, Int. J. Fatigue 32. DOI: 10.1016/j.ijfatigue.2009.07.009

Stach, S., Sapota, W., Ţălu, Ş., Ahmadpourian, A., Luna, C., Ghobadi, N., Arman, A., Ganji, M., 2017. *3-D surface stereometry studies of sputtered TiN thin films obtained at different substrate temperatures*, J. Mater. Sci. Mater. Electron. DOI: 10.1007/s10854-016-5774-9

Stemp, W.J., Macdonald, D.A., Gleason, M.A., 2019. *Testing imaging confocal microscopy, laser scanning confocal microscopy, and focus variation microscopy for microscale measurement of edge cross-sections and calculation of edge curvature on stone tools: Preliminary results*, J. Archaeol. Sci. Reports 24, 513-525. DOI: 10.1016/J.JASREP.2019.02.010

Susmel, L., Petrone, N., 2003. *Multiaxial fatigue life estimations for 6082-T6 cylindrical specimens under in-phase and out-of-phase biaxial loadings*, Eur. Struct. Integr. Soc. 31, 83-104. DOI: 10.1016/S1566-1369(03)80006-7

Szala, M., 2017. *Application of computer image analysis software for determining incubation period of cavitation erosion – preliminary results*, ITM Web Conf. 15 06003 DOI: 10.1051/itmconf/20171506003

Trško, L., Lago, Ján, Jambor, M., Nový, F., Bokůvka, O., Florková, Z. 2020. *Microstructure and residual stress analysis of Strenx 700 MC welded joint*, Production Engineering Archives, 26(2), 41-44. DOI: 10.30657/pea.2020.26.09

Ulewicz, R., Nový, F., Novák, P., Palček, P., 2019. *The investigation of the fatigue failure of passenger carriage draw-hook*, Eng. Fail. Anal. 104, 609-616. DOI: 10.1016/j.engfailanal.2019.06.036

Ulewicz, R., Szataniak, P., Novy, F. 2014. *Fatigue Properties Of Wear Resistant Martensitic Steel*, Metal 2014 - 23rd International Conference on Metallurgy and Materials, Conference Proceedings

Vanderesse, N., Texier, D., Bocher, P., 2020. *Effect of porosities on brazed martensitic steel tensile properties: 2D and 3D pre-mortem vs post-mortem characterizations*, Mater. Charact. 160, 110084. DOI: 10.1016/J.MATCHAR.2019.110084

Wu, Q., Liu, X., Liang, Z. et al. 2020. *Fatigue life prediction model of metallic materials considering crack propagation and closure effect*, J Braz. Soc. Mech. Sci. Eng. 42, 424. DOI: 10.1007/s40430-020-02512-1

Yang, D., Xiao, X., Liu, Y., & Sun, J., 2019. *Peripheral milling-induced residual stress and its effect on tensile–tensile fatigue life of aeronautic titanium alloy Ti–6Al–4V*, The Aeronautical Journal, 123(1260), 212-229. DOI: doi:10.1017/aer.2018.151

非零平均应力弯曲扭转疲劳对34CrNiMo6缺口钢板断裂表面参数的影响

關鍵詞
多轴疲劳 弯曲扭转 缺口效应 疲劳断裂 表面形貌

摘要
现代的材料测试方法要求使用最新技术，并结合测量和计算方法。找到定量描述故障的方法很重要，这样它可以帮助进行高精度设计。本文研究了裂纹形状和断裂表面变化的加载方向。整个断裂面方法的优点是在研究其他材料，形状和载荷方面简单易行。在具有较低σ/τ（B / T）比的破坏样本中观察到较高的断裂表面参数（Sx，Vx）值。已经观察到，与B = T不同的载荷组合会出现具有少量循环的最大裂纹长度。对于较大数量的裂纹起始（Ni）值循环，分析的表面参数Sx，Vx也会更高。